J Ther Eng, Vol. 11, No. 1, pp. 127−140, January, 2025

Journal of Thermal Engineering
Web page info: https://jten.yildiz.edu.tr
DOI: 10.14744/thermal.0000908

Research Article

Numerical analysis of nanofluid flow over a radiating oscillating plate with hall current and MHD at enhanced temperature

S. SARALA[1,2,*], E. GEETHA[1]

[1]*Department of Mathematics, Sri Chandrasekharendra Saraswathi Viswa Maha Vidyalaya, Tamil Nadu, 631561, India*
[2]*Department of Mathematics, Paavai Engineering College (Autonomous), Tamil Nadu, 637018, India*

ARTICLE INFO

Article history
Received: 16 October 2023
Revised: 15 April 2024
Accepted: 23 April 2024

Keywords:
Alumina; Radiation; Magnetic Field Parameter; Primary Velocity; Secondary Velocity; Variable Temperature

ABSTRACT

The study investigates the impact of various factors, including magnetohydrodynamics (MHD), alumina nanofluid flow, thermal radiation, Hall current, and harmonic oscillations on convective heat generation at enhanced temperatures on a plate. The plate experiences harmonic oscillations while maintaining a uniform temperature, and dimensional equations are converted into non-dimensional ones using specific parameters. Through Laplace transformation, an exact solution is derived. Analysis of velocity and temperature considers the Prandtl number, Grashof number, Hall parameter, magnetic parameter, radiation, solid volume fraction, and phase angle. Graphs illustrate the impact of primary and secondary velocity, showing increased velocities with higher Grashof numbers and decreased velocities with rising Hall parameters. Moreover, the temperature rises in line with the solid volume fraction. Effective heat transfer is crucial for improving energy efficiency in industrial processes, HVAC (heating, ventilation, and air conditioning) systems, and thermal management setups. Engineers utilize the Nusselt number to optimize heat transfer equipment design. For instance, at Nu = 0.9258 (at t = 0.5, Pr = 0.71, solid volume fraction = 0.26, R = 1). and In magnetohydrodynamics (MHD), the presence of a magnetic field alters the fluid flow behavior. At higher magnetic field strengths, the fluid flow becomes more constrained or influenced by the magnetic forces, which can lead to increased frictional resistance along the surface of the plate. The skin friction coefficient values increase for both velocities as the magnetic field parameter reaches 4, 5, and 6. Graphical representations of mathematical findings enhance comprehension of temperature and velocity variations, emphasizing the importance of heat transfer efficiency.

Cite this article as: Sarala S, Geetha E. Numerical analysis of nanofluid flow over a radiating oscillating plate with hall current and MHD at enhanced temperature. J Ther Eng 2025;11(1):127−140.

***Corresponding author.**
*E-mail address: geethamuthu06@gmail.com

This paper was recommended for publication in revised form by Editor-in-Chief Ahmet Selim Dalkılıç

Published by Yıldız Technical University Press, İstanbul, Turkey

INTRODUCTION

Heat transmission analysis depends on interactions between dimensionless parameters. The objective of heat transfer in nanofluids is to enhance the thermal performance of the fluid compared to traditional heat transfer fluids.

Research continues on the use of nanofluids in cooling systems, such as for industrial heat exchangers, automobile engines, and electronic devices. These systems benefit from improved heat removal efficiency due to increased thermal conductivity. The Hall Effect is a phenomenon in physics named after the American physicist Edwin Hall, who first described it in 1879. This effect refers to the generation of a voltage (hall voltage) across an electrical conductor transverse to the electric current and an applied magnetic field. Many electronic devices, including magnetic encoders, position sensors, and speed sensors, as well as sensors like Hall effect sensors, which are used to measure magnetic fields and detect current, make extensive use of the Hall effect. The Hall Effect is particularly significant in the study of semiconductors and metals, and it has various practical applications. The Hall impact is caused by the characteristics of an electric current flowing through a conductor. Electricity has tiny moving charge transporters such as electrons, holes, ions, or jointly. The Hall response sensor is a typical instrument used to measure the potency of a magnetic field. It detects the Hall current, which is caused by an electric current flowing through a conductor. Hall current is applied to the MHD power generator, magnetic field sensing equipment, phase angle measurement, sensors with their probes, wheel speed detection, and accordingly assists the anti-lock braking system. Improved heat dissipation, decreased thermal resistance, higher thermal conductivity, the potential for smaller heat exchangers, and energy efficiency are the main goals of employing nanofluids in heat transfer applications. The nanofluid model typically used is a single-phase model, where the nanofluid is treated as a homogeneous mixture of nanoparticles dispersed within a base fluid. This approach assumes that the nanoparticles are well-dispersed and uniformly distributed throughout the fluid, leading to a single-phase flow behavior. Assumptions for the nanofluid model include homogeneous dispersion of nanoparticles within the fluid, assuming stable suspension techniques to prevent aggregation or settling. It also assumes negligible particle-particle interactions compared to interactions with the base fluid, simplifying the model. Nanoparticles are assumed to rapidly reach thermal equilibrium with the fluid due to their high surface area-to-volume ratio. Nanoparticles in a nanofluid experience Brownian motion, which is the random movement of particles suspended in a fluid due to collisions with solvent molecules. This motion causes the nanoparticles to disperse throughout the fluid, enhancing the thermal conductivity and convective heat transfer properties of the nanofluid. The interaction between nanoparticles and the base fluid also influences the thermal behavior of the nanofluid. Surface chemistry, intermolecular forces, and the stability of the colloidal suspension can all affect the dispersion and thermal properties of the nanofluid. Additionally, properties such as density, viscosity, and thermal conductivity are presumed constant across temperature and nanoparticle concentration ranges, though exceptions may occur under extreme conditions. Nanofluids are the latest exciting growing technology that is helping to raise the thermal conductivity of liquids. Nanofluids exist in microelectronics, fuel cells, pharmaceutical industry. Alumina nanofluid enforces greater thermal conductivity.

In their analysis, Roy et al. [1] applied three methods to solve equations based on their frequency ranges. Based on a study by Muthucumaraswamy [2], it was found that the velocity in a vertical oscillating plate with a chemical reaction decreased as the phase angle increased while keeping the concentration constant and varying the temperature. Nagarajan et al. [3] intended radiation effects along with chemical reactions and it plays a vital role in health and military forces. Sridhara et al. [4] gave importance to the coolant to control thermal expansion. Ilyas Khan et al. [5] noted that temperature and concentration variations gave way to driving forces from thermal diffusion. Murali Gundagani et al. [6] used a finite element solution. When exploring the possibilities of using nanofluids in renewable energy sources, Omid Mahian et al. [7] examined both the benefits and challenges of this approach. They also evaluated the effectiveness of a nanofluid-based direct absorption solar collector, taking into account factors such as measurement of the dimension and volumetric proportion of nanoparticles used.

Loganathan et al. [8] calculated the heat transfer rate using four distinct types of nanofluids. This investigation appears to be relevant to the field of chemical reactions and heat transport. He established that Silver water nanofluid had the best heat transfer rate with radiation compared to other nanofluid. Muthucumaraswamy et.al [9] discussed various applications for MHD in this context. The Laplace transformation is widely employed to solve governing equations. Chandrakala et al. [10] discussed the effects of oscillating plates with radiation at a constant temperature. She believed in the importance of thermal radiation effects except that not getting more attention from researchers. Abid Hussanan et al. [11] insisted on Newtonian heating which neglects inner resistance compared to surface resistance. Okedoye [12] used a combination of sub-methods including the Richardson extrapolation technique, along with Fehlberg's fourth-fifth order Runge-Kutta shooting iteration method by degree four interpolant to solve the governing equations. Rajesh et al. [13] examined the influence of nanofluid flow on moving vertical plates with temperature oscillation possessions with radiation. Murali et al. [14] solved the governing equations using the Galerkin finite element method. Many practical diffusive processes involve the molecular diffusion of a species in the presence of a chemical reaction occurring within or at the boundary, as noted by Babu et al. [15]. For this reason, engineers and

scientists find it extremely useful to analyze heat and mass transport in chemical reactions.

Ahmad Qushairi Mohamad et al. [16] introduced non-coaxial spin in convection flow, as it has been proven to be useful for stirring, cooling turbine blades, and even vacuum cleaners. Bayomy et al. [17] examined the extreme relative error of the Nusselt number and local experimental temperature and concluded that the uniformity index was 68% less valuable to using water as the coolant substitute for air. Gauri Shankar Seth et al. [18] were concerned about the consequences of Hall current and convective flow of rotating fluid along ramped wall temperature and revealed that MHD-free convective flow is applied in many industries for high-temperature forming. Rajput et al. [19] studied the heat immersion on flow prototypical along variable temperature and also observed that both velocity decrement because of increment immersion and angle. In their study, Sonia Nasrin et al. [20] related infinite Oscillating porous plate along Hall current and found thermal and concentration flux with persistent temperature. Jithender Reddy et al. [21] utilized the Casson fluid model to determine the viscous dissipation in the presence of an oscillating vertical plate. They were able to obtain a solution by implementing the finite element method. Iqbal et al. [22] probed the influences of a radiative hybrid nanofluid along the Hall current in an oscillating vertical plate. Jithender Reddy et al.

Tokgoz et al. [23] took the corrugated duct, instead of the smooth duct to evaluate heat transfer enhancement in channel flow, and flow properties of an alumina-water nanofluid through corrugated channels with varying geometric shapes were explored numerically. Vijayalakshmi et al. [24] applied the Runge-Kutta method to solve differential equations and analyzed the statistical variations of skin friction, thermal, and concentration transfer coefficients. It's fascinating to see how different methods can be applied to solve complex equations and lead to insightful findings. Manjula et al. [25] considered an inclined radiative oscillating plate and found the responses of Dufour number. Shantha Sheela et al. [26] reviewed an overview of the magnetohydrodynamic flow of nanofluids via a vertical plate with radiation and numerical schemes are found to be more favorable than analytical schemes because of the intricacy of the governing equations. Kanif Markad et al. [27] investigated the impact of multi-walled carbon nanotube (MWCNT) modification on shape memory polymer hybrid composites, focusing on their mechanical, thermomechanical, and shape memory properties. Arulmozhi et al. [28] deliberated reactions in moving radiative infinite vertical plate existence of chemicals. Aamir Farooq et al. [29] examined the Maxwell Nanofluid's oscillatory behavior concerning mass and heat transport. Engine oil is used as a base fluid and graphene nanoparticles are added to it because of its high heat conductivity. Kanif et al.[30] observed that increasing the thickness of piezoelectric layers led to a significant rise in voltage, while the total thickness of the laminated plate remained unchanged. Kanif Markad et al.[31] discussed that the fabrication process involves preparing the SMPHC through magnetic stirring, shear mixing, and ultrasonication, followed by molding using the hand layup method. Stefan Heidinger et al.[32] compared the 33 sets of correlations and data points from both simulations and experiments, a meta-correlation has been derived for calculating the Nusselt number. Markad Kanif et al. [33] highlighted the crucial role of carbon nanotubes, multi-wall carbon nanotubes, graphene, and nano-silica in the development of nanocomposites. Mehboob Ali et al. [34] applied a conversion technique to solve the dimensionless equations, followed by employing the numerical approach Bvp4c for their solution. Aamir Ali et al. [35] expanded our comprehension of fluid dynamics and heat transfer in intricate systems. Investigating how magnetic effects, nanofluid characteristics, and heat conduction interact allows researchers to make substantial progress in fluid mechanics and heat transfer. Understanding Hall effects holds particular importance in applications with conductive fluids or plasma, as they provide a more precise understanding of the behavior of charged nanoparticles in the presence of a magnetic field. Yuchi Leng et al. [36] found that fluid flow dynamics are influenced by porous media, magnetic fields, and fluid properties, while heat transfer is affected by factors such as Eckert number, magnetic effects, and thermophoresis. Additionally, fluid absorption is influenced by activation energy and Brownian motion. These principles have applications across various industries including medicine, pharmacology, and chemistry, and are also relevant in food processing, particularly through Joule heating. Design considerations such as streamlines, heat lines, and mass lines play a critical role in optimizing processes. Muhammad Aqib Aslam et al. [37] investigated that while heat and mass transfer rates peak with shear-thinning fluids, they diminish with shear-thickening fluids. Additionally, they observed that these rates are highest in concentration-dominated assistant flow and lowest in concentration-dominant counter flow. Based on the literature review, they discussed the convective heat transfer, numerous boundary conditions, and varieties of special fluids, radiation, and vertical oscillating plates. Here Alumina is considered as a nanofluid and water is a base fluid.

As far as our comprehension extends, there have been no inquiries undertaken regarding the influence of magnetohydrodynamic (MHD) nanofluid flow over an oscillating vertical plate with enhanced temperature, taking into account Hall effects and radiation.

MATHEMATICAL ANALYSIS

The viscosity of an incompressible Al_2O_3 nanofluid has been examined when it passes by a vertical plate that oscillates while thermal radiation is present. The temperature of the plate and fluid is the same at the time $t^* \leq 0$, or T_∞. Along the x^* axis, the plate has oscillated, and for the remaining axes, the y^* axis is normal. Initially, the plate has the temperature T_∞ When it starts to oscillate, the temperature of the plate is raised to T_w. z^* axis is uniformly paralleled by the

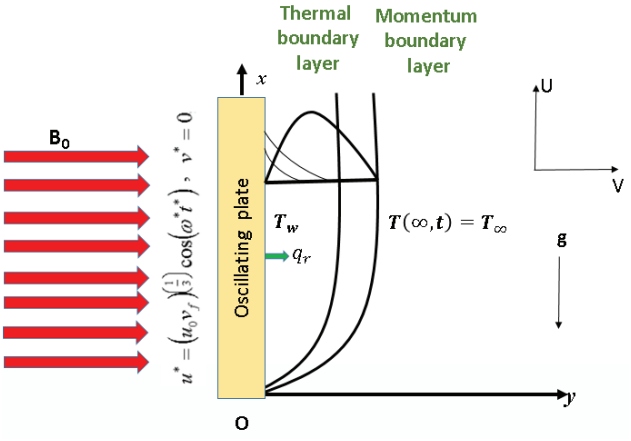

Figure 1. The geometry of a problem.

uniform magnetic field B_0. The usual direction of application of the radiative heat flux (q_r) to the plate is observed. An indestructible behavior of Al_2O_3 nanofluid as it flows over an oscillating plate in the existence of thermal radiation has been studied. The problem's geometry is in Figure 1.

The equation $z^*= 0$ and the x^*oy^* a plane is considered. The plate's temperature and the fluid's temperature are identical at the time $t^* \le 0$. The oscillations of the plate along the x^* and the y^* axes and remaining axes are normal to the plate. The starting velocity of Oscillating is $u^* = (u_0 v_f)^{(\frac{1}{3})} \cos(\omega^* t^*)$ an increase in temperature T_w. The z^* axis is parallel to the uniform magnetic field B_0, which is applied uniformly. The plate receives the radiative heat flux q_r in the usual direction. The thermo physical properties of water and alumina nanoparticles are listed in Table 1, and Figure 1 shows the actual model.

The elements $\vec{F}$ are indicated by the letters u*, v*, and w* in $\nabla \cdot \vec{F} = 0$ and w*=0. The velocity similarity variables are used as the main similarity variables in this pseudo-similarity transformation. It is indicated by η. The usage of water-based Al_2O_3 nanoparticles as a fluid is considered. The suspended nanoparticles, which are in thermal equilibrium, are transported with the base fluid. Z* and t* control the flow. The uninterrupted flow further from the plate is taken into account. In the far field, far away from the plate, the velocity boundary condition is often set to a specified value, representing the bulk flow conditions of the fluid far from the influence of the plate. Similarly, the temperature boundary condition in the far field is usually prescribed as a constant value, reflecting the ambient conditions or the conditions at the outlet of the system. These boundary conditions provide the necessary constraints to solve the governing equations for the fluid flow and heat transfer within the domain of interest, ensuring that the behavior of the nanofluid is appropriately modeled both near the solid surface and in the far field.

The formula for the following unsteady flow represents the equations that govern the Boussinesq's approximation:

$$\rho_{nf} \frac{\partial u^*}{\partial t^*} = \mu_{nf} \frac{\partial^2 u^*}{\partial z^{*2}} + g(\rho\beta)_{nf}(T - T_\infty) + \frac{\sigma_{nf} B_0^2 \left(m v^* - u^*\right)}{\left(1 + m^2\right)} \quad (1)$$

$$\rho_{nf} \frac{\partial v^*}{\partial t^*} = \mu_{nf} \frac{\partial^2 v^*}{\partial z^{*2}} - \frac{\sigma_{nf} B_0^2 \left(v^* + m u^*\right)}{\left(1 + m^2\right)} \quad (2)$$

$$(\rho c_p)_{nf} \frac{\partial T}{\partial t^*} = k_{nf} \frac{\partial^2 T}{\partial z^{*2}} - \frac{\partial q_r}{\partial z^*} \quad (3)$$

where u* and v* are the primary and secondary velocities. Eq. (1), and Eq. (2) are momentum equations and Eq. (3) is an energy equation.

The necessary boundary constraints are

$$\begin{array}{llll} u^* = 0, & v^* = 0, & T = T_\infty, & for\ all\ z^*, t^* \le 0 \\ u^* = (u_0 v_f)^{(\frac{1}{3})} \cos(\omega^* t^*), & v^* = 0, & T = T_\infty + (T_w - T_\infty) A t^*, & for\ all\ t^* > 0, z^* = 0 \\ u^* \to 0, & v^* \to 0, & T \to T_\infty & at\ z^* \to \infty \end{array} \quad (4)$$

Where $A = \left(\frac{u_0^2}{v_f}\right)^{(\frac{1}{3})}$

The introduced non-dimensional quantities are as follows:

$$U = \frac{u^*}{(u_0 v_f)^{(\frac{1}{3})}}, \quad V = \frac{v^*}{(u_0 v_f)^{(\frac{1}{3})}},$$

$$Z = z^* \left(\frac{u_0}{v_f^2}\right)^{(\frac{1}{3})}. \quad \omega = \omega^* \left(\frac{v_f}{u_0^2}\right)^{(\frac{1}{3})}$$

$$t = t^* \left(\frac{u_0^2}{v_f}\right)^{(\frac{1}{3})}, \quad \theta = \frac{T - T_\infty}{T_w - T_\infty}$$

$$Gr = \frac{g \beta_f (T_w - T_\infty)}{u_0}$$

$$R = \frac{16\, a^*\, \sigma_f T_\infty^{\,3}}{k_f} \left(\frac{v_f^{\,2}}{u_0}\right)^{(\frac{1}{3})}$$

$$\Pr = \frac{\mu c_p}{k_f}$$

$$M^2 = \frac{\sigma_f B_0^2}{\rho_f} \left(\frac{v_f}{u_0^{\,2}}\right)^{(\frac{1}{3})}$$

Table 1. Thermo-physical properties of water and Alumina nanoparticles

Physical Properties	ρ (kg / m^3)	C_p (J/KgK)	K(W / mK)	$\beta \times 10^5$ (K^{-1})	ϕ	σ(S/m)
Water / Base Fluid	997.1	4179	0.613	21	0.0	5.5 x 10^{-6}
Al_2O_3 (Alumina)	3970	765	40	0.85	0.15	35 x 10^6

$$\frac{\partial q_r}{\partial z^*} = -4a^* \sigma_f \left(T_\infty^4 - T^4\right) \tag{5}$$

The temperature changes within the flow are presumably minimal enough to be described as a linear function of temperature. To do this, higher-order terms are not taken into account when expanding in a Taylor series, so

$$T^4 \cong 4T_\infty^3 T - 3T_\infty^4 \tag{6}$$

Equation (3) for the dimensionless parameter reduces to

$$(\rho c_p)_{nf} \frac{\partial T}{\partial t'} = k_{nf} \frac{\partial^2 T}{\partial z^{*2}} + 16a^* \sigma T_\infty^3 (T_\infty - T) \tag{7}$$

When the dimensionless parameters are employed in Eq. (1), Eq. (2), and Eq. (3) produce the following equations

$$L_1 \frac{\partial U}{\partial t} = L_3 \frac{\partial^2 U}{\partial Z^2} + L_4 \frac{(U - mV)M^2}{1+m^2} + L_2 Gr.\theta \tag{8}$$

$$L_1 \frac{\partial V}{\partial t} = L_3 \frac{\partial^2 V}{\partial Z^2} - L_4 \frac{(mU + V)M^2}{1+m^2} \tag{9}$$

$$L_5 \frac{\partial \theta}{\partial t} = L_6 \frac{1}{\Pr} \frac{\partial^2 \theta}{\partial Z^2} - \frac{R}{\Pr}\theta \tag{10}$$

Where

$$L_1 = (1-\phi) + \phi\left(\frac{\rho_s}{\rho_f}\right)$$

$$L_2 = (1-\phi) + \phi\left(\frac{(\rho\beta)_s}{(\rho\beta)_f}\right)$$

$$L_3 = \frac{1}{(1-\phi)^{2.5}}$$

$$L_4 = 1 + \frac{3(\sigma-1)\phi}{(\sigma+2)-(\sigma-1)\phi}, \qquad \sigma = \frac{\sigma_s}{\sigma_f}$$

$$L_5 = (1-\phi) + \phi\left(\frac{(\rho c_p)_s}{(\rho c_p)_f}\right)$$

$$L_6 = \left[\frac{k_s + 2k_f - 2\phi(k_f - k_s)}{k_s + 2k_f + \phi(k_f - k_s)}\right]$$

Eq. (11), which represents the relevant beginning and boundary conditions

$$t>0: \begin{array}{lll} U=0, & V=0, & \theta=0 \quad for\ all \quad Z,t\le 0 \\ U=Cos(\omega t), & V=0, & \theta=t \quad at \quad Z=0 \\ U\to 0, & V\to 0, & \theta\to 0 \ at \quad Z\to\infty \end{array} \tag{11}$$

$$LetF = U + iV \tag{12}$$

$$L_1 \frac{\partial F}{\partial t} = L_3 \frac{\partial^2 F}{\partial Z^2} - L_4 \frac{F(1+im)M^2}{1+m^2} + L_2 Gr.\theta$$

The most recent equations are

$$L_1 \frac{\partial F}{\partial t} = L_3 \frac{\partial^2 F}{\partial Z^2} - L_4 F b_1 + L_2 Gr.\theta \tag{13}$$

$$L_5 \frac{\partial \theta}{\partial t} = L_6 \frac{1}{\Pr} \frac{\partial^2 \theta}{\partial Z^2} - \frac{R}{\Pr}\theta \tag{14}$$

The most recent beginning and boundary conditions are,

$$t>0: \begin{array}{lll} F=0, & \theta=0 \ for\ all\ Z,t\le 0 \\ F=Cos(\omega t), & \theta=t \quad at \quad Z=0 \\ F\to 0, & \theta\to 0 \ at \quad Z\to\infty \end{array} \tag{15}$$

Solution Procedure

The complementary and exponential error functions are used to express the solution. As an indication of the relationship between the error function and its complementary error function,

$$erfc(x) = 1 - \mathrm{erf}(x) \tag{16}$$

The main dimensionless equations Eq. (13) and Eq. (14) as well as the conditional equation Eq. (15) are solved using the conventional Laplace transformation. Following is an explanation of the findings.

$$\begin{aligned} F = {} & \frac{\exp(i\omega t)}{4}\left(\begin{array}{l}\exp(2\eta\sqrt{g(b_2+i\omega)t})\ erfc\left(\eta\sqrt{g}+\sqrt{(b_2+i\omega)t}\right) \\ +\exp(-2\eta\sqrt{g(b_2+i\omega)t})\ erfc\left(\eta\sqrt{g}-\sqrt{(b_2+i\omega)t}\right)\end{array}\right) \\ & + \frac{\exp(-i\omega t)}{4}\left(\begin{array}{l}\exp(2\eta\sqrt{g(b_2-i\omega)t})\ erfc\left(\eta\sqrt{g}+\sqrt{(b_2-i\omega)t}\right) \\ +\exp(-2\eta\sqrt{g(b_2-i\omega)t})\ erfc\left(\eta\sqrt{g}-\sqrt{(b_2-i\omega)t}\right)\end{array}\right) \\ & - \frac{c.\exp(dt)}{2d^2}\left(\begin{array}{l}\exp\left(2\eta\sqrt{g(b_2+d)t}\right)erfc\left(\eta\sqrt{g}+\sqrt{(b_2+d)t}\right) \\ +\exp\left(-2\eta\sqrt{g(b_2+d)t}\right)erfc\left(\eta\sqrt{g}-\sqrt{(b_2+d)t}\right)\end{array}\right) \\ & + \frac{c}{2d^2}\left(\exp\left(2\eta\sqrt{gb_2t}\right)erfc\left(\eta\sqrt{g}+\sqrt{b_2t}\right)+\exp\left(-2\eta\sqrt{gb_2t}\right)erfc\left(\eta\sqrt{g}-\sqrt{b_2t}\right)\right) \\ & + \frac{ct}{2d}\left(\exp\left(2\eta\sqrt{Rt}\right)erfc\left(\eta\sqrt{g}+\sqrt{b_2t}\right)+\exp\left(-2\eta\sqrt{Rt}\right)erfc\left(\eta\sqrt{g}-\sqrt{b_2t}\right)\right) \\ & - \frac{c\eta g\sqrt{t}}{2d\sqrt{R}}\left(\exp\left(-2\eta\sqrt{Rt}\right)erfc\left(\eta\sqrt{g}-\sqrt{b_2t}\right)-\exp\left(2\eta\sqrt{Rt}\right)erfc\left(\eta\sqrt{g}+\sqrt{b_2t}\right)\right) \\ & + \frac{c.\exp(dt)}{2d^2}\left(\begin{array}{l}\exp\left(2\eta\sqrt{a(b+d)t}\right)erfc\left(\eta\sqrt{a}+\sqrt{(b+d)t}\right) \\ +\exp\left(-2\eta\sqrt{a(b+d)t}\right)erfc\left(\eta\sqrt{a}-\sqrt{(b+d)t}\right)\end{array}\right) \\ & - \frac{c}{2d^2}\left(\exp\left(2\eta\sqrt{abt}\right)erfc\left(\eta\sqrt{a}+\sqrt{bt}\right)+\exp\left(-2\eta\sqrt{abt}\right)erfc\left(\eta\sqrt{a}-\sqrt{bt}\right)\right) \\ & - \frac{ct}{2d}\left(\exp\left(2\eta\sqrt{Rt}\right)erfc\left(\eta\sqrt{a}+\sqrt{bt}\right)+\exp\left(-2\eta\sqrt{Rt}\right)erfc\left(\eta\sqrt{a}-\sqrt{bt}\right)\right) \\ & + \frac{\eta ac\sqrt{t}}{2d\sqrt{R}}\left(\exp\left(-2\eta\sqrt{Rt}\right)erfc\left(\eta\sqrt{a}-\sqrt{bt}\right)-\exp\left(2\eta\sqrt{Rt}\right)erfc\left(\eta\sqrt{a}+\sqrt{bt}\right)\right) \end{aligned} \tag{17}$$

$$\begin{aligned} \theta = {} & \frac{t}{2}\left(\exp(2\eta\sqrt{Rt})\ erfc\left(\eta\sqrt{a}+\sqrt{bt}\right)+\exp(-2\eta\sqrt{Rt})\ erfc\left(\eta\sqrt{a}-\sqrt{bt}\right)\right) \\ & - \frac{\eta a\sqrt{t}}{2\sqrt{R}}\left(\exp\left(-2\eta\sqrt{Rt}\right)erfc\left(\eta\sqrt{a}-\sqrt{bt}\right)-\exp\left(2\eta\sqrt{Rt}\right)erfc\left(\eta\sqrt{a}+\sqrt{bt}\right)\right) \end{aligned} \tag{18}$$

Where $a = \frac{L_5 \Pr}{L_6}$, $b = \frac{R}{L_5 \Pr}$, $b_1 = \frac{M^2(1+im)}{1+m^2}$, $b_2 = \frac{L_4 b_1}{L_1}$,

$$c = \frac{L_2 Gr}{L_1 - L_3 a}, \quad d = \frac{L_3 ab - L_4 b_1}{L_1 - L_3 a}$$

Eq. (17) denoted the velocity and Eq. (18) represented temperature.

$$C_f = -\left(\frac{\partial F}{\partial \eta}\right)_{\eta=0} \tag{19}$$

$$Nu = -\left(\frac{\partial \theta}{\partial \eta}\right)_{\eta=0} \tag{20}$$

According to Eq. (19) and Eq. (20), the Skin friction coefficient and Nusselt number, respectively, are terms used to refer to the derivative of F and θ with beginning conditions.

$$erf(a+ib) = erf(a) + \frac{\exp(-a^2)}{2a\pi}[1-\cos(2ab)+i\sin(2ab)] + \frac{\exp(-a^2)}{\pi}\sum_{n=1}^{\infty}\frac{\exp\left(\frac{-n^2}{4}\right)}{n^2+4a^2}[f_n(a,b)+ig_n(a,b)]+\in(a,b)$$

Where $f_n = 2a - 2a\cosh(nb)\cos(2ab) + n\sinh(nb)\sin(2ab)$

$g_n = 2a\cosh(nb)\sin(2ab) + n\sinh(nb)\cos(2ab)$

$|\in(a,b)| \approx 10^{-16}|erf(a+ib)|$

The complex error function is separated into its real (U) and imaginary (V) components using the formula above.

RESULTS AND DISCUSSION

Numerical calculations for various physical factors Gr, R, M, m, ω, ϕ and t depending on dynamics and transportation are taken into consideration to interpret the results for a better analysis of the problem. The numerical values of the velocity and temperature are computed for the parameters Gr, R, M, m, t, and ϕ.

Effects of Different Parameters on the Primary and Secondary Velocity Profile

A decline in U and V (velocity components) in Figures 2 and 10 gradually decreases in the region far away as the magnetic field parameter (M) is increased due to the influence of the magnetic field on the fluid flow. As the magnetic field parameter increases, the magnetic forces become stronger. These magnetic forces act on the fluid, causing it to resist motion perpendicular to the magnetic field lines. Consequently, the velocity components U and V decrease gradually as the magnetic field parameter increases, particularly in regions far away from the source of the magnetic field. This is because the plate, which has a stronger hydromagnetic body force, has a stronger hydromagnetic field. The main velocity U in Figure 9 was reduced by increasing ω from π/30 to π/2, and V in Figure 17 was also reduced. One possible explanation could be that at higher angular frequencies, the flow becomes more constrained or directed in a certain manner, leading to a reduction in overall fluid velocities U and V within the system. Additionally, increased angular frequency might induce greater fluid resistance or turbulence, resulting in reduced velocities. Figures 4 and 12 show how the U and V rise as the value of the Grashof number (Gr) increases and how this occurs for flow control. When the Grashof number increases, the buoyancy forces induce stronger convective motion within the fluid. This enhanced convective motion leads to increased fluid velocities, both in the main direction (U) and tangential direction (V), as shown in Figures 4 and 12. A dimension of the boundary layer expansion is the major aspect of the Prandtl number. Both of the velocities in Figures 5 and 13 increase

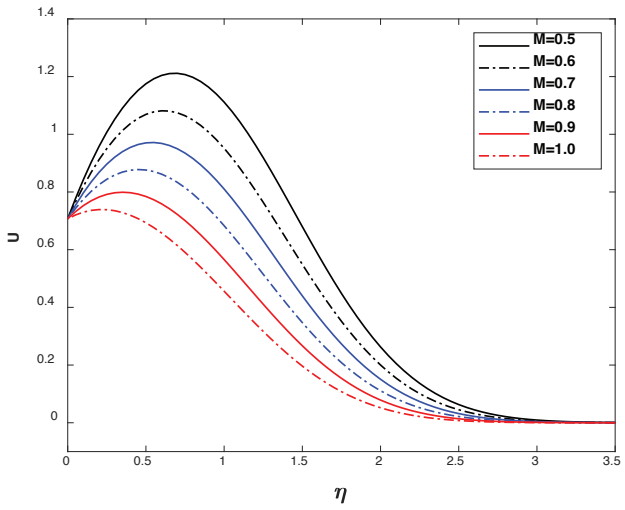

Figure 2. Distinct M values for U.

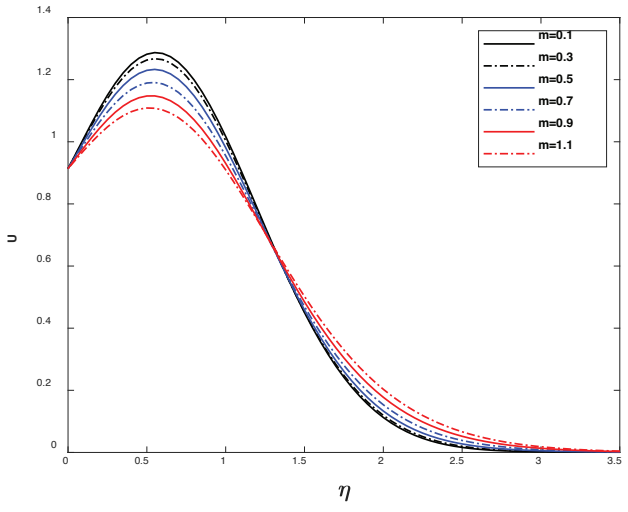

Figure 3. Distinct m values for U.

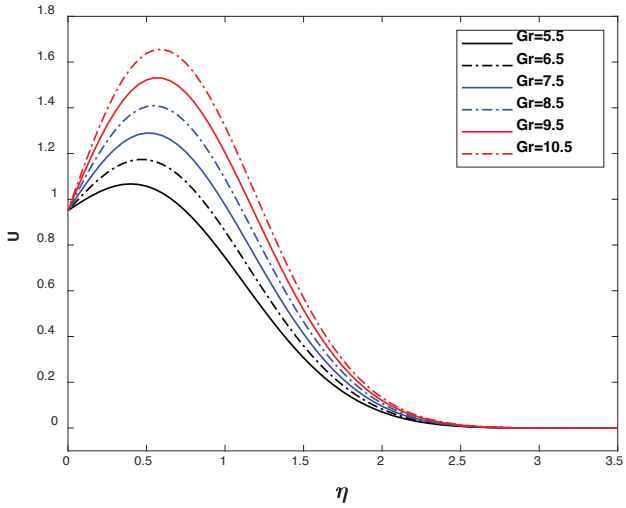

Figure 4. Distinct Gr values for U.

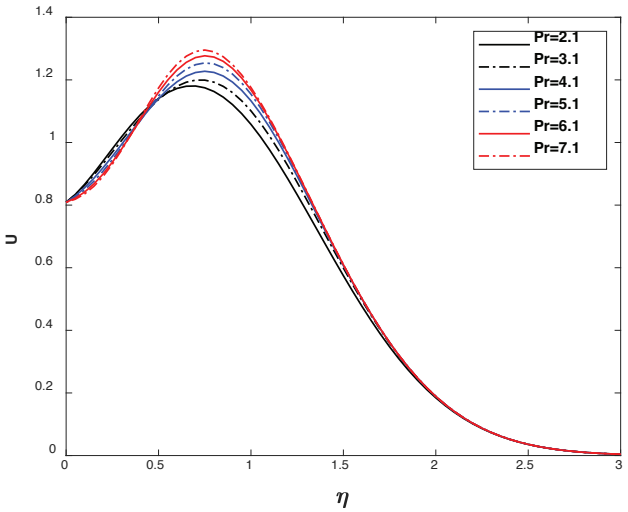

Figure 5. Distinct Pr values for U.

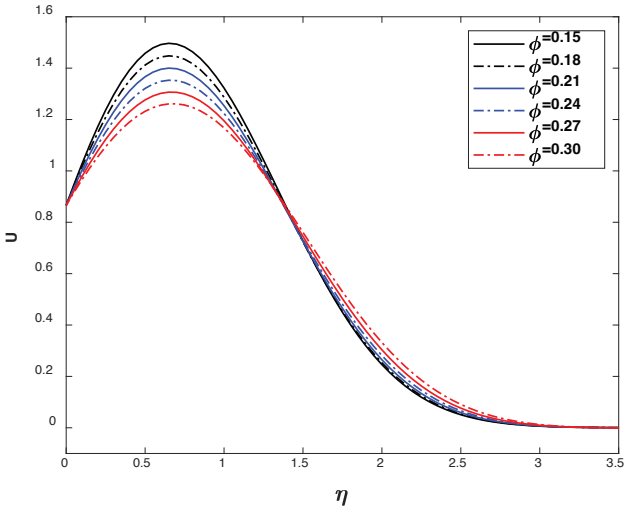

Figure 6. Distinct ϕ values for U.

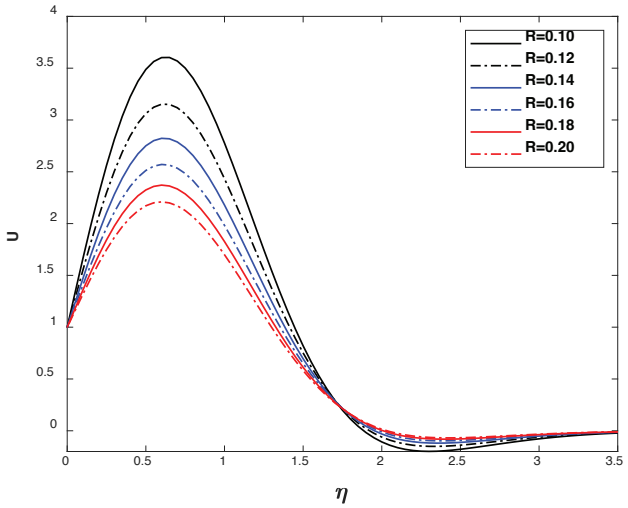

Figure 7. Distinct R values for U.

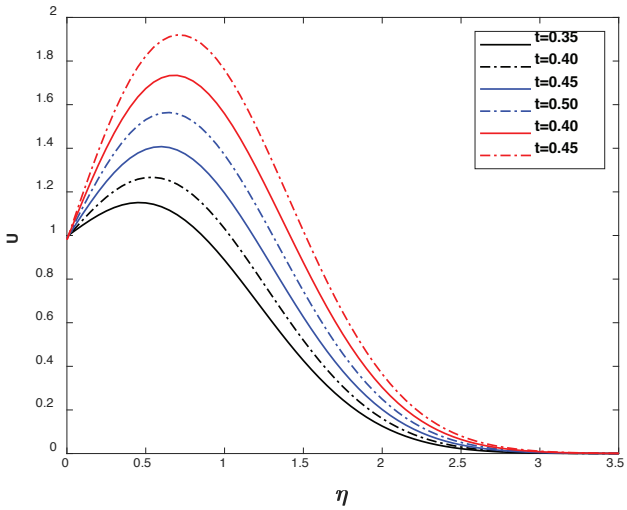

Figure 8. Distinct t values for U.

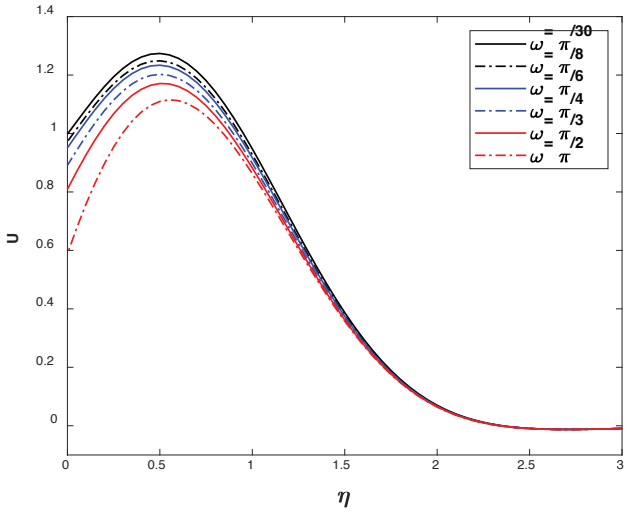

Figure 9. Distinct ω values for U.

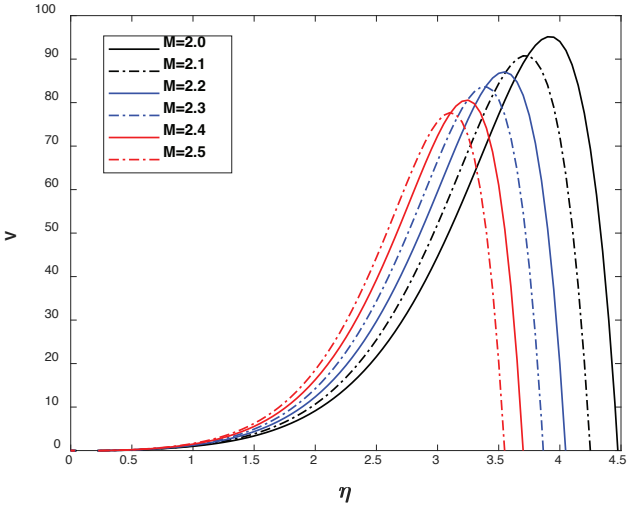

Figure 10. Distinct M values for V.

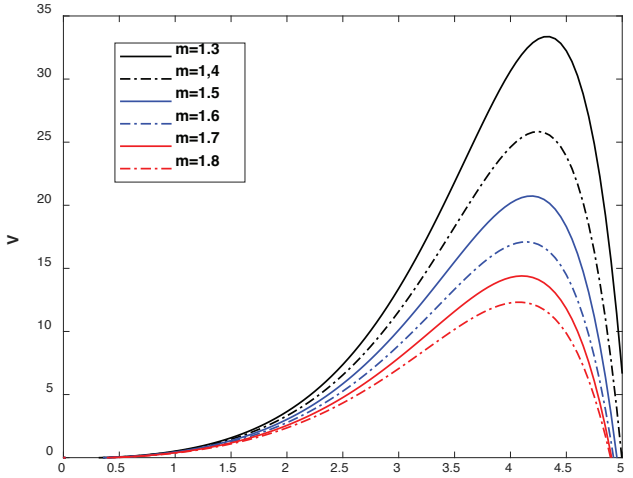

Figure 11. Distinct m values for V.

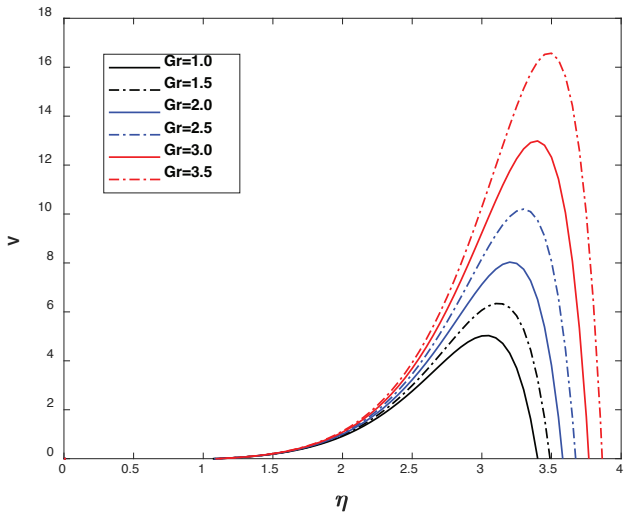

Figure 12. Distinct Gr values for V.

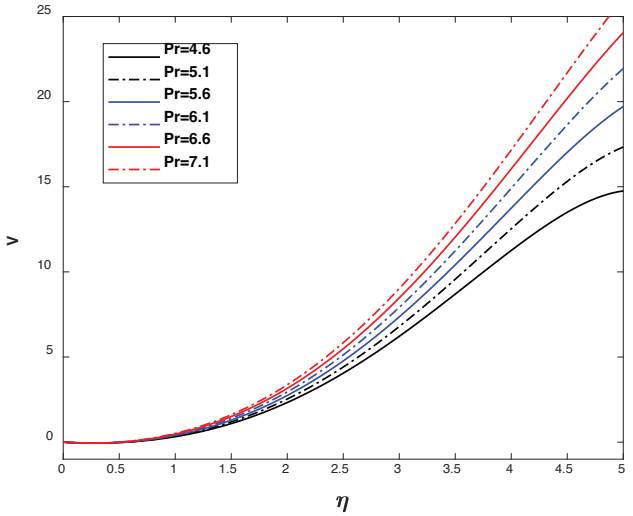

Figure 13. Distinct Pr values for V.

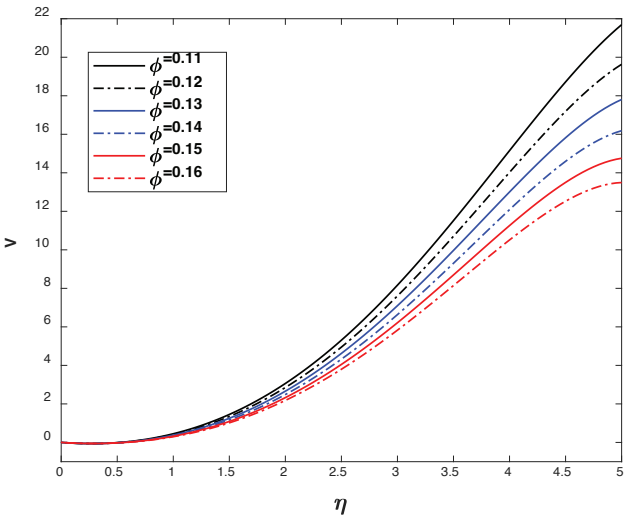

Figure 14. Distinct ϕ values for V.

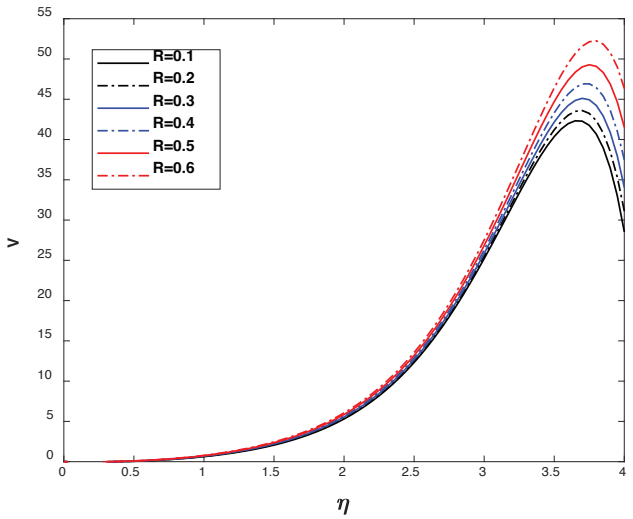

Figure 15. Distinct R values for V.

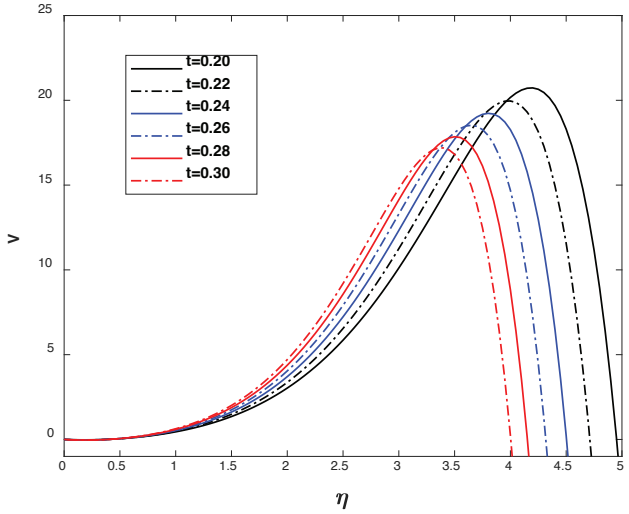

Figure 16. Distinct t values for V.

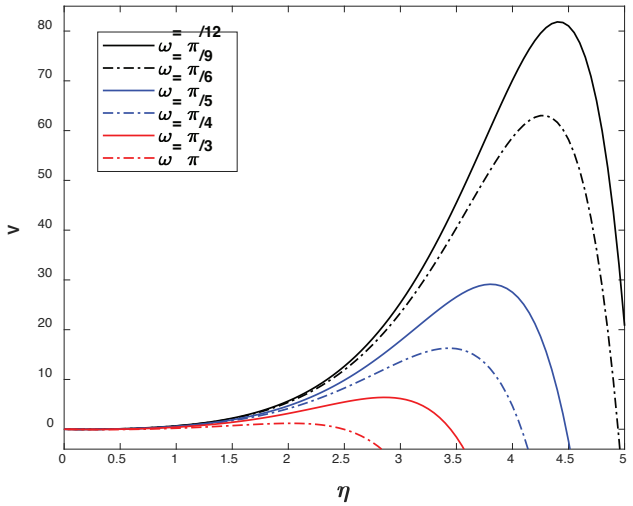

Figure 17. Distinct ω values for V.

as the Prandtl number rises. The increase in both velocities (U and V) with rising Prandtl number can be attributed to the influence of the Prandtl number on the boundary layer thicknesses, which in turn affects heat transfer rates and fluid motion within the boundary layer.

The ϕ increment causes the U and V in Figures 6 and 14 to decrease. Particles with a larger mass increment weigh more and study about diminish in velocity. The primary velocity U in Figure 7 is decreased and V in Figure 15 rises as a result of the radiation increase. Because of how quickly the fluid moves with oscillations. Figure 8 shows an increase in primary velocity U for an ascending value of time (t), and Figure 16 shows a reversal of the trend in secondary velocity V. Figure 3 shows that U fell when the value of the Hall parameter (m) was raised, while Figure 11 shows that the V trended in the same direction.

Temperature Profile Parameter Exploration

In Figure 18, the temperature decreases as the solid volume fraction increases due to weight because a higher solid volume fraction implies a greater mass of solid particles within the system. As a result, more thermal energy is absorbed by the increased mass of solid particles, leading to a reduction in the overall temperature of the system. Thermophoresis refers to the movement of particles in response to a temperature gradient. In a nanofluid, this phenomenon can cause the nanoparticles to migrate toward regions of higher or lower temperature depending on the specific characteristics of the particles and the fluid. This movement can affect the distribution of nanoparticles within the fluid and consequently influence its thermal behavior. In Figure 19. increment of Pr values leads to a decrease in the temperature. To lower the temperature thermal diffusivity, add the Prandtl number values together. In the temperature profile, the most specific parameter is

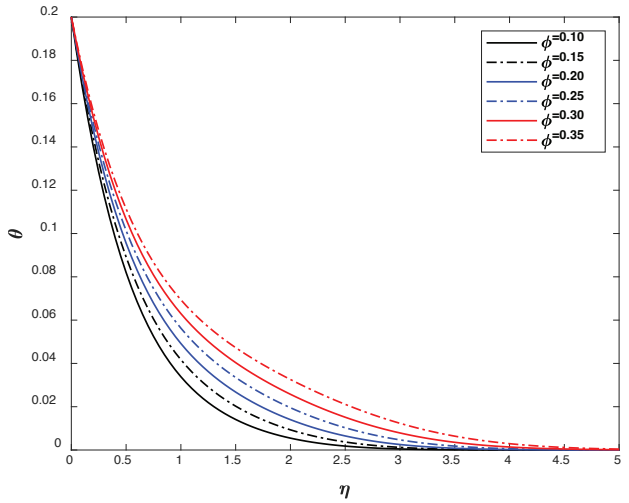

Figure 18. Variations in temperature using various ϕ values.

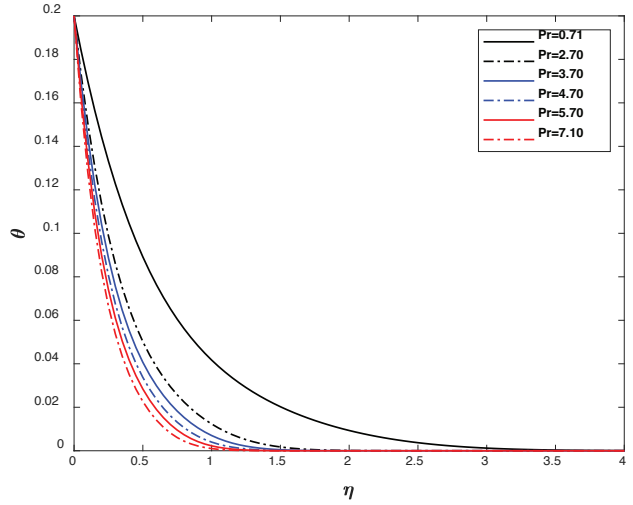

Figure 19. Variations in temperature using various Pr values.

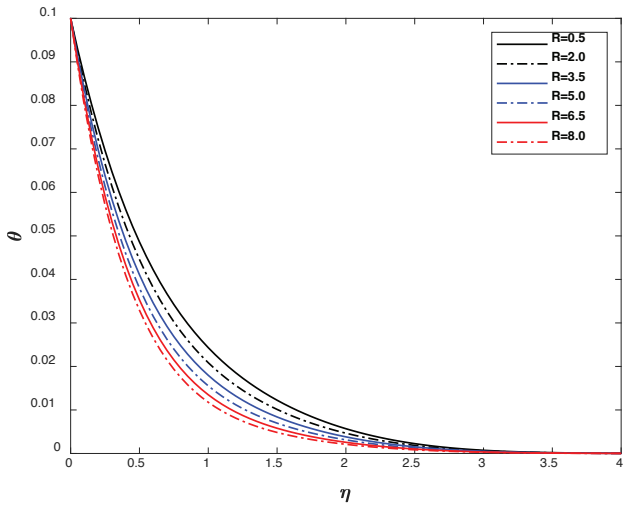

Figure 20. Variations in temperature using various R values.

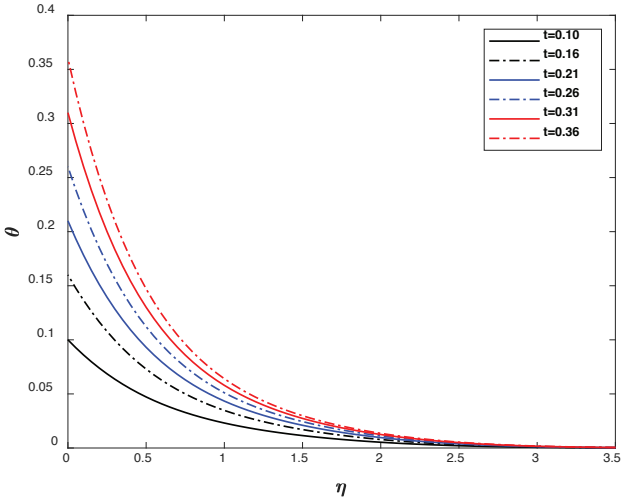

Figure 21. Variations in temperature using various t values.

radiation, and noted that an increment of radiation leads to a decrease the temperature in Figure 20.

For a choice of t = 0.10, 0.16, 0.21, and 0.26, 0.31, 0.36, the temperature variations are shown in Fig 21. and because of improved temperature boundary conditions, each unit of time results in a temperature rise. Enhanced temperature boundary conditions may minimize heat loss from the system to the surroundings, preserving more thermal energy within the system and contributing to a continuous temperature rise.

Exploration of Nu & C_f

In Table 2, various values of solid volume fraction, R, Pr, and t are considered and enumerated. The relative contributions of convective and conductive heat transport are shown by the magnitude of the Nusselt number, a dimensionless quantity. Convective heat transmission is predominant when the Nusselt number is large, but conductive heat transfer is more important when the Nusselt number is low.

Table 2. Variations of Nusselt values

t	Pr	ϕ	R	$-\theta'(0)$
0.1	0.71	0.15	0.7	0.1408
0.4	0.71	0.15	0.7	0.7053
0.9	0.71	0.15	0.7	2.0375
0.2	**1.7**	0.15	0.5	0.4031
0.2	**4.3**	0.15	0.5	0.6103
0.2	**6.8**	0.15	1	0.7581
0.5	0.71	**0.11**	1	1.0185
0.5	0.71	**0.26**	1	0.9258
0.5	0.71	**0.31**	1	0.8549
0.1	0.71	0.15	**0.5**	0.1323
0.1	0.71	0.15	**1.5**	0.1629
0.1	0.71	0.15	**2.5**	0.1784

Table 3. Modifications to the Nusselt number

Pr	Ref.[3]	Present Study
0.71	0.5461	0.4492
1.0	0.7692	0.4986
7.1	5.3846	1.1271

Tabulate the Nusselt numbers calculated from simulations for different nanoparticle volume fractions or Prandtl numbers. This table provides insights into how these parameters influence the heat transfer rate from the plate to the fluid. By comparing numerical results with existing analytical solutions or benchmark cases, researchers can validate the accuracy of their computational models for alumina nanofluid and gain confidence in their predictive capabilities. Additionally, any discrepancies between numerical and analytical results can provide insights into the limitations of the computational approach and guide further improvements in the modeling techniques used.

The Nusselt numbers are listed in Table 3 and Figure 22 and Figure 23, increments of t and R direct to increase the Nusselt number. Convective heat transmission is predominant when the Nusselt number is large, but conductive heat transfer is more important when the Nusselt number is low.

The latest research paper likely shows improved phase angle results due to advanced experimental or computational techniques enhancing measurement accuracy. Refinement of parameters to better reflect real-world conditions and updated material property data, especially heat and mass transfer coefficients, could have significantly influenced the outcomes.

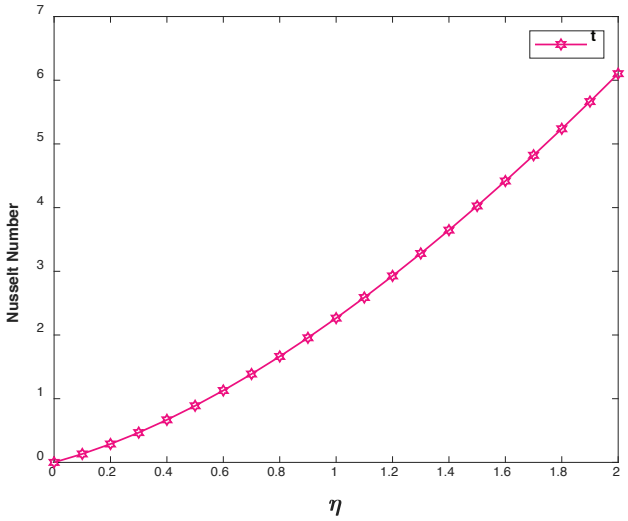

Figure 22. Nusselt number values for various t.

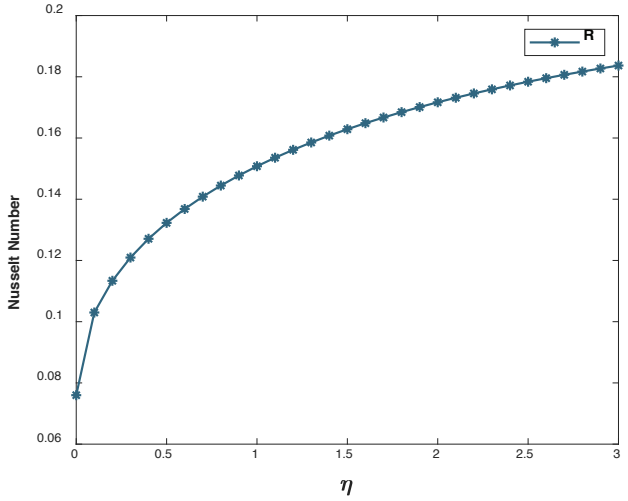

Figure 23. Nusselt number values for various R.

Table 4. Differences between U and V›s skin friction coefficient values

t	ϕ	Pr	R	M	Gr	ω	m	C_f (Primary)	C_f (Secondary)
0.3								1.5836	0.5075
0.5	0.15	0.71	1	2	5	π/3	1	1.6471	1.0139
0.9								1.1367	2.1822
	0.16							1.6439	0.7331
0.4	**0.29**	0.71	1	2	5	π/3	1	1.6285	0.6089
	0.43							1.5275	0.5274
		2.1						1.7370	0.5007
0.3	0.15	**5.1**	1	2	5	π/3	1	1.6505	0.2121
		7.1						1.6096	0.2938
			1.2					1.6737	1.0376
0.5	0.15	0.71	**1.4**	2	5	π/3	1	1.6935	1.0686
			1.6					1.7083	1.1062
				4				3.7494	1.7759
0.6	0.15	0.71	1	**5**	5	π/3	1	4.7750	2.1555
				6				5.7851	2.5516
					6			1.6144	0.7934
0.4	0.15	0.71	1	2	**8**	π/3	1	1.5583	0.8849
					10			1.5023	0.9764
						π/6		2.2126	1.3893
0.7	0.15	0.71	1	2	5	**π/4**	1	1.9058	1.4775
						π/2		0.4310	1.8405
							0.5	1.6453	0.1788
0.2	0.15	0.71	1	2	5	π/3	**2.0**	1.2509	0.4225
							3.0	1.1386	0.5223

Table 5. Contrasting the outcomes of skin friction coefficient (C_f)

ω	Rajput et al.		current study	
	Across U	Across V	Across U	Across V
π/6	8.46596	-1.16007	1.7239	0.8630
π/4	8.30705	-1.16017	1.6307	0.9109
π/3	8.09995	-1.16028	1.5023	0.9764

Current study values are positive and positive skin friction values indicate that the shear stress acts in the same direction as the flow of the fluid. This means that the fluid is exerting a force on the surface in the direction of the flow. Several variables, including surface roughness and flow characteristics, affect the skin friction coefficient in Table 5. In other contexts, negative skin friction values indicate that the shear stress acts opposite to the direction of the fluid flow. This means that the surface is exerting a resistive force on the fluid, opposite to the flow direction. To minimize skin friction and reduce drag, it is frequently employed in the analysis of boundary layer flow over surfaces, such as aircraft wings. Note that the skin friction coefficient might have several different formulations based on the particulars of the flow under consideration and the context in which it is used. MATLAB has calculated the C_f values of the U and V and listed them in Table 3 for a variety of values of ϕ, t, Pr, R, ω, M, and m. Skin friction in V lowers in value over time. Additionally, it has been found that skin friction gets progressively less as M gets larger.

CONCLUSION

Radiative oscillating vertical plates at various temperatures have been explored accompanied by MHD and Hall current. The Hall Effect combined with nanofluids that have magnetic nanoparticles can potentially boost and regulate heat transfer in thermal systems. It seems like manipulating the magnetic field could influence the distribution of the nanoparticles and maximize heat transfer efficiency. Magnetic nanofluids have proven to be very useful in biomedical applications, especially for targeted drug delivery. The Hall Effect is a phenomenon that can be used to guide and direct these magnetic nanofluids to specific locations within the body. By applying an external magnetic field, the nanofluids can be precisely directed to the desired location, which can help to increase the effectiveness of drug delivery while minimizing potential side effects. Utilizing the Laplace-transform approach, equations are resolved. For both U and V, the possessions of various parameters Gr, Pr, t, R, M, m, and solid volume fraction are visually explored. The Skin Friction Coefficient and the Nusselt number are investigated with different numerical values. There are so many different types of nanoparticles out there that could be used to create new and improved nanofluids. Future research work may be performed using new and improved Nanofluids. Following are the conclusions reached by the current study.

- The velocity in the primary and secondary flow increases as the Prandtl number and Grashof number are increased. In contrast, the solid volume particle, Hall parameter, magnetic field parameters, and phase angle are reversed. Increases in time, increase in primary velocity, and a decrease in secondary velocity because of oscillations with increased hotness.
- As the radiation parameter and Prandtl parameter have higher values, the fluid's temperature falls. However, because of its large size and stronger boundary conditions, increasing the solid volume particle and time results rise in temperature.
- The ranges of the Nusselt numbers grow with increasing values of t, Pr, and R, but decrease with increasing values of the solid volume fraction.
- For the rise in phase angle, the skin friction values in primary velocity increased and secondary velocity reduced.

NOMENCLATURE

A	Constant
α	Thermal diffusivity
B_0	Constant applied magnetic
β	Thermal expansion coefficient
C_p	Specific heat at constant pressure
C_f	Coefficient of Skin Friction
E	Electric field
ε	Dimensionless small quantity
η	Pseudo-similarity variable
F	Complex Function
g	Gravity acceleration
Gr	Thermal Grashof number
k	Thermal conductivity
M	Dimensionless magnetic field parameter
m	Hall Parameter
Nu	Nusselt Number
ω	Phase angle
Pr	Prandtl number
ρ	Density
ϕ	The solid volume fraction of the nanoparticles
$\bar{q}_w$	Dimensional heat flux from the plate
R	Radiation
σ	Electrical conductivity
$t\text{^}\star$	Time
t	Dimensionless time
T	Local temperature of the nanofluid
T_w	Wall temperature
T_∞	The temperature of the ambient nanofluid
θ	Kinematic viscosity
$u^\star, v^\star, w^\star$	Velocity components along $x^\star$, $y^\star$, $z^\star$axes
U, V, W	Dimensionless velocity components
μ	Dynamic viscosity
ϑ	Kinematic viscosity
x, y, z	Cartesian coordinates

ACKNOWLEDGMENTS

The authors would like to thank the respectful reviewers for their constructive comments.

AUTHORSHIP CONTRIBUTIONS

S. Sarala: wrote the first version of the manuscript; methodology; prepared the figures; and contributed to answering comments. E. Geetha: supervision; review and editing; validation; interpreted the results and contributed to answering the comments.

DATA AVAILABILITY STATEMENT

The authors confirm that the data that supports the findings of this study are available within the article. Raw data that support the finding of this study are available from the corresponding author, upon reasonable request.

CONFLICT OF INTEREST

The authors declared no potential conflicts of interest with respect to the research, authorship, and/or publication of this article.

ETHICS

There are no ethical issues with the publication of this manuscript.

REFERENCES

[1] Roy N, Hossain MA. The effect of conduction-radiation on the oscillating natural convection boundary layer flow of viscous incompressible fluid along a vertical plate. Proc Inst Mech Eng Part C J Mech Eng Sci 2010;224:1959–1972. [CrossRef]

[2] Muthucumaraswamy R. Chemical reaction effects on vertical oscillating plate with variable temperature. Chem Ind Chem Eng Q 2010;16:167–173. [CrossRef]

[3] Nagarajan G, Sundar Raj M. First order chemical reaction on MHD flow past an oscillating vertical plate in the presence of thermal radiation. Int J Appl Mech Eng 2011;16:1081–1091.

[4] Sridhara V, Satapathy LN. Al2O3-based nanofluids: A review. Nanoscale Res Lett 2011;6:1–16. [CrossRef]

[5] Khan I, Fakhar K, Shafie S. Magnetohydrodynamic free convection flow past an oscillating plate embedded in a porous medium. J Phys Soc Jpn 2011;80:1–10. [CrossRef]

[6] Gundagani M, Sivaiah S, Babu NVN, Reddy MCK. Finite element solution of thermal radiation effect on unsteady MHD flow past a vertical porous plate with variable suction. Am Acad Sch Res J 2012;4:1–12. [CrossRef]

[7] Mahian O, Kianifar A, Kalogirou SA, Pop I, Wongwises S. A review of the applications of nanofluids in solar energy. Int J Heat Mass Transf 2013;57:582–594. [CrossRef]

[8] Loganathan P, Chand PN, Ganesan P. Radiation effects on an unsteady natural convective flow of a nanofluid past an infinite vertical plate. Nano 2013;8:1–10. [CrossRef]

[9] Muthucumaraswamy R, Geetha E. Chemical reaction effects on MHD flow past a linearly accelerated vertical plate with variable temperature and mass diffusion in the presence of thermal radiation. Int J Appl Mech Eng 2013;18:727–737. [CrossRef]

[10] Chandrakala P, Bhaskar PN. Radiation effects on oscillating vertical plate with uniform heat and mass flux. Int J Appl Mech Eng 2013;18:643–652. [CrossRef]

[11] Hussanan A, Anwar MI, Ali F, Khan I, Shafie S. Natural convection flow past an oscillating plate with Newtonian heating. Heat Transf Res 2014;45:119–135. [CrossRef]

[12] Okedoye AM. Unsteady MHD mixed convection flow past an oscillating plate with heat source/sink. J Nav Archit Mar Eng 2014;11:167–176. [CrossRef]

[13] Rajesh V, Mallesh MP, Sridevi C. Transient MHD nanofluid flow and heat transfer due to a moving vertical plate with thermal radiation and temperature oscillation effects. Procedia Eng 2015;127:901–908. [CrossRef]

[14] Murali G, Paul NB. Heat and mass transfer effects on an unsteady hydromagnetic free convective flow over an infinite vertical plate embedded in a porous medium with heat absorption. Int J Open Probl Compt Math 2015;8:15–27. [CrossRef]

[15] Babu NVN, Paul A, Murali G. Soret and Dufour effects on unsteady hydromagnetic free convective fluid flow past an infinite vertical porous plate in the presence of chemical reaction. J Sci Arts 2015;1:99–111.

[16] Mohamad AQ, Khan I, Ismail Z, Shafie S. Exact solutions for unsteady free convection flow over an oscillating plate due to non-coaxial rotation. Springerplus 2016;5:1–13. [CrossRef]

[17] Bayomy AM, Saghir MZ, Yousefi T. Electronic cooling using water flow in aluminum metal foam heat sink: Experimental and numerical approach. Int J Therm Sci 2016;109:182–200. [CrossRef]

[18] Seth GS, Bhattacharyya A, Tripathi R. Effect of Hall current on MHD natural convection heat and mass transfer flow of rotating fluid past a vertical plate with ramped wall temperature. Front Heat Mass Transf 2017;9:1–12. [CrossRef]

[19] Rajput US, Kumar G. Effect of heat absorption on MHD flow over a plate with variable wall temperature. J Appl Sci Eng 2017;20:277–282.

[20] Nasrin S, Islam R, Alam M. MHD heat and mass transfer on viscoelastic fluid flow through an infinite

oscillating porous plate in the presence of Hall current with constant heat and mass flux. J Sci Eng Res 2018;5:52–64.
[21] Reddy GJ, Raju RS, Rao JA. Influence of viscous dissipation on unsteady MHD natural convective flow of Casson fluid over an oscillating vertical plate via FEM. Ain Shams Eng J 2018;9:1907–1915. [CrossRef]
[22] Iqbal Z, Akbar NS, Azhar E, Maraj EN. Performance of hybrid nanofluid (Cu-CuO/water) on MHD rotating transport in oscillating vertical channel inspired by Hall current and thermal radiation. Alexandria Eng J 2018;57:1943–1954. [CrossRef]
[23] Tokgoz N, Aliç E, Kaska, Aksoy MM. The numerical study of heat transfer enhancement using Al2O3-water nanofluid in corrugated duct application. J Therm Eng 2018;4:1984–1997. [CrossRef]
[24] Vijayalakshmi K, Umadevi RM, Muthucumaraswamy R. Oscillating plate in nanofluid with uniform heat and mass flux under the effect of MHD, radiation and chemical reaction analyzed by Runge-Kutta method. Taga J 2018;14:793–803.
[25] Manjula V, Sekhar KVC. Effects of Hall current, Dufour on unsteady MHD chemically reacting Casson fluid flow over an inclined oscillating plate with thermal radiation. Int J Sci Technol Res 2020;9:6439–6452.
[26] Shanthasheela J, Gururaj ADM, Ismail M, Dhanasekar S. Review on magnetohydrodynamic flow of nanofluids past a vertical plate under the influence of thermal radiation. IOP Conf Ser Earth Environ Sci 2021;850:012037. [CrossRef]
[27] Markad K, Lal A. Experimental investigation of shape memory polymer hybrid nanocomposites modified by carbon fiber reinforced multi-walled carbon nanotube (MWCNT). Mater Res Express 2021;8:105015. [CrossRef]
[28] Arulmozhi S, Sukkiramathi K, Santra SS, Edwan R, Fernandez-Gamiz U, Noeiaghdam S. Heat and mass transfer analysis of radiative and chemical reactive effects on MHD nanofluid over an infinite moving vertical plate. Results Eng 2022;14:100394. [CrossRef]
[29] Farooq A, Rehman S, Alharbi AN, Kamran M. Closed-form solution of oscillating Maxwell nanofluid with heat and mass transfer. Sci Rep 2022;12:1–13. [CrossRef]
[30] Markad K, Das V, Lal A. Deflection and stress analysis of piezoelectric laminated composite plate under variable polynomial transverse loading. AIP Adv 2022;12:085024. [CrossRef]
[31] Markad K, Lal A. Synthesis of the multiphase shape memory hybrid composites hybridized with functionalized MWCNT to improve mechanical and interfacial properties. Polym Plast Technol Mater 2022;61:650–664. [CrossRef]
[32] Heidinger S. Heat and mass transfer to particles in one-dimensional oscillating flows. Processes 2023;11:1–15. [CrossRef]
[33] Kanif M, Vivek P, Kishor K. Structural analysis of nano-filler based structural composite. J Aeronaut Mater 2023;43:188–202.
[34] Ali M, Pasha AA, Nawaz R, Khan WA, Irshad K, Algarni S, Alqahtani T. Innovation modeling and simulation of thermal convective on cross nanofluid flow over exponentially stretchable surface. Heliyon 2023;9:e18672. [CrossRef]
[35] Ali A, Khan HS, Noor I, Pasha AA, Irshad K, Al Mesfer MK, Danish M. Hall effects and Cattaneo–Christov heat flux on MHD flow of hybrid nanofluid over a varying thickness stretching surface. Mod Phys Lett B 2023;37:1–13. [CrossRef]
[36] Leng Y, Li S, Algarni S, Jamshed W, Alqahtani T, Ibrahim RW, Irshad K, ElSeabee FAA, Hassan AM. Computational study of magnetized and dual stratified effects on non-Darcy Casson nanofluid flow: An activation energy analysis. Case Stud Therm Eng 2024;53:103804. [CrossRef]
[37] Aslam MA, Yao H, Al Mesfer MK, Shahzad H, Danish M, Irshad K. Numerical analysis of double-diffusive natural convective flow of Ostwald-de Waele fluid in an irregular enclosure with a circular obstacle. Results Phys 2024;56:107312. [CrossRef]